NeuroImage 52 (2010) 1559–1573

Contents lists available at ScienceDirect

NeuroImage

journal homepage: www.elsevier.com/locate/ynimg

Sparsely-distributed organization of face and limb activations in human ventral temporal cortex

Kevin S. Weiner [a,*], Kalanit Grill-Spector [a,b]

[a] Department of Psychology, Stanford University, Stanford, CA 94305, USA
[b] Neuroscience Institute, Stanford University, Stanford, CA 94305, USA

ARTICLE INFO

Article history:
Received 2 December 2009
Revised 9 April 2010
Accepted 29 April 2010
Available online 10 May 2010

Keywords:
fMRI
Ventral stream
Fusiform
Object recognition
Human extrastriate cortex

ABSTRACT

Functional magnetic resonance imaging (fMRI) has identified face- and body part-selective regions, as well as distributed activation patterns for object categories across human ventral temporal cortex (VTC), eliciting a debate regarding functional organization in VTC and neural coding of object categories. Using high-resolution fMRI, we illustrate that face- and limb-selective activations alternate in a series of largely nonoverlapping clusters in lateral VTC along the inferior occipital gyrus (IOG), fusiform gyrus (FG), and occipito-temporal sulcus (OTS). Both general linear model (GLM) and multivoxel pattern (MVP) analyses show that face- and limb-selective activations minimally overlap and that this organization is consistent across experiments and days. We provide a reliable method to separate two face-selective clusters on the middle and posterior FG (mFus and pFus), and another on the IOG using their spatial relation to limb-selective activations and retinotopic areas hV4, VO-1/2, and hMT+. Furthermore, these activations show a gradient of increasing face selectivity and decreasing limb selectivity from the IOG to the mFus. Finally, MVP analyses indicate that there is differential information for faces in lateral VTC (containing weakly- and highly-selective voxels) relative to non-selective voxels in medial VTC. These findings suggest a sparsely-distributed organization where sparseness refers to the presence of several face- and limb-selective clusters in VTC, and distributed refers to the presence of different amounts of information in highly-, weakly-, and non-selective voxels. Consequently, theories of object recognition should consider the functional and spatial constraints of neural coding across a series of minimally overlapping category-selective clusters that are themselves distributed.

Introduction

Recent findings from functional magnetic resonance imaging (fMRI) studies indicate that human ventral temporal cortex (VTC) contains regions responding more strongly to faces or body parts relative to other objects (Kanwisher et al., 1997; Peelen and Downing, 2005; Pinsk et al., 2009; Schwarzlose et al., 2005), as well as discriminable distributed activation patterns for object categories across VTC (Haxby et al., 2001). As a result, there is an ongoing debate regarding the spatial organization and function of these regions (Grill-Spector, 2003).

One view of functional organization in VTC suggests a modular organization whereby there is a domain-specific region for processing faces (fusiform face area, FFA) and another domain-specific region for processing body parts (fusiform body area, FBA) and these regions do not overlap (Schwarzlose et al., 2005). This view has been refined over the last decade in a series of reviews (Kanwisher, 2000; Op de Beeck et al., 2008; Peelen and Downing, 2007a,b). However, there are several outstanding issues. First, the modular view does not make particular predictions about the size of these regions, only that they are larger than a cortical column (Op de Beeck et al., 2008). Second, this view is particularly appealing if there is only one (or few) region(s) dedicated to specialized computations for a handful of categories that require unique processing. Third, if these face- and body part-selective activations are distinct brain areas dedicated for specific computations, these areas should be spatially arranged in a consistent manner similar to the organization of early visual areas, where there is a consistent anatomical location and consistent spatial relationship relative to other visual areas. However, there are inconsistencies across studies regarding (1) whether or not face- and body part-selective regions overlap (Peelen and Downing, 2005; Pinsk et al., 2009; Schwarzlose et al., 2005), (2) if there is one or more than one face- and body part-selective region in VTC (Peelen and Downing, 2005; Pinsk et al., 2009; Schwarzlose et al., 2005), and (3) whether or not there is a consistent spatial relationship between face- and body part-selective activations.

These inconsistencies are due in part by the assumption that there are a definitive number of face-selective activations. For example, the standard model of face processing suggests three core face-selective regions in the occipital and temporal lobes (Haxby et al., 2000): a region in the fusiform gyrus (FFA) dedicated for face detection and identification (Andrews et al., 2002; Grill-Spector et al., 2004; Hasson

* Corresponding author.
E-mail address: kweiner@stanford.edu (K.S. Weiner).

1053-8119/$ – see front matter © 2010 Elsevier Inc. All rights reserved.
doi:10.1016/j.neuroimage.2010.04.262

et al., 2001; Tong et al., 1998), a region in the inferior occipital gyrus (typically referred to as the occipital face area, OFA; Gauthier et al., 2000), and a region in the posterior superior temporal sulcus (pSTS) thought to be involved in processing dynamic aspects of faces such as emotion and gaze (Andrews and Ewbank, 2004; Engell and Haxby, 2007; Haxby et al., 2000; Ishai et al., 2000; Puce et al., 1998). Thus, using general linear model (GLM) analyses, researchers usually label face-selective (as compared to objects) activations on the fusiform gyrus (FG) as the FFA, even when these activations are split into two separate clusters (e.g. Grill-Spector et al., 2004). However, in some studies when the OFA is absent, the anterior FG cluster is labeled as the FFA and the posterior FG cluster is labeled as the OFA even when the activation is clearly on the posterior FG (e.g. Tsao et al., 2008). Likewise, any FG or occipito-temporal sulcus (OTS) activation for the visual presentation of bodies and/or limbs compared to objects is labeled as the FBA, regardless of its overlap with the FFA or its precise location relative to the FFA. While this ventral temporal body part-selective activation tends to be reported lateral to face-selective activations (Peelen and Downing, 2005; Pinsk et al., 2009; Schwarzlose et al., 2005), there is variability in its location: sometimes it is reported anterior to the FFA, while other times posterior to the FFA. This variation in location is reported within the same study at standard resolution (Peelen and Downing, 2005), high-resolution (Schwarzlose et al., 2005), and even when attempting to separate both the FFA and FBA into separate clusters (Pinsk et al., 2009). The inconsistent spatial relation between face- and limb-selective activations violates one of the principles for parcellating cortex into areas (Felleman and Van Essen, 1991). If we use retinotopic divisions as a guide, researchers always delineate V2v between V1 and V3v, as there is a consistent organization of these areas relative to one another. Consequently, an open question remains if there is a consistent fine-scale organization among VTC regions, which may have been overlooked due to a combination of prior imaging and analysis methods.

An alternate view of functional organization in VTC suggests a highly overlapping and distributed organization for faces, limbs, and objects. This view is supported by evidence that different categories generate different distributed response patterns (referred to as multivoxel patterns, MVP) across VTC (Cox and Savoy, 2003; Edelman et al., 1998; Haxby et al., 2001). Further support for this view comes from evidence that MVPs across VTC contain information about object categories and faces even when excluding category-selective regions (Haxby et al., 2001), and that activations for faces and body parts in VTC overlap which suggests a common region for processing these stimuli (Peelen and Downing, 2005; Peelen et al., 2006). However, as with the modular view, there are outstanding issues. First, MVP analyses tend to ignore the spatial organization of category information across VTC, and only measure whether or not activations are informative. Second, while research indicates that there is category information in MVPs both inside and outside category-selective regions (Grill-Spector et al., 2006; Hanson and Halchenko, 2008; Haxby et al., 2001; Sayres and Grill-Spector, 2008; Schwarzlose et al., 2008; Spiridon and Kanwisher, 2002), there is no coherent answer as to whether there is equal information across highly-, weakly-, and non-selective voxels. Third, this view does not attempt to explain why there are clusters of selectivity for some categories, but not others (e.g. there does not seem to be a brain region dedicated for processing cars, but see Gauthier et al., 2000).

While traditionally the GLM approach is used to define regions of selectivity and MVP analyses ignore spatial organization, MVP analyses can also be used to elucidate the spatial and functional organization in VTC (Downing et al., 2007; Peelen et al., 2006). These MVP analyses can elucidate, for example, whether face- and body part-selective activations in VTC are overlapping or distinct. One concern using the GLM approach to address this question is that the outcome may depend on the analysis steps, especially whether or not the data are spatially smoothed and the threshold used to define the activations. If data are spatially smoothed and low thresholds are used, activations may appear overlapping, but if there is no spatial smoothing and a high threshold is used, activations may appear distinct.

Here we propose that MVP analyses can also be used to examine the spatial organization of distributed responses both across as well as outside category-selective regions with the advantage that the results are threshold independent (Peelen and Downing, 2007a,b). If we find that MVPs for faces and limbs across VTC are anticorrelated, it would indicate that distinct subsets of VTC voxels respond preferentially to faces and limbs. Such a finding would be consistent with the modular view if the anticorrelation between MVPs is driven by category-selective regions. However, if GLM analyses reveal overlapping face- and limb-selective regions, it does not necessarily mean that there is a common representation of faces and limbs because there are two possible outcomes. One possibility is that MVPs to faces and limbs are positively correlated, which means that voxels preferring faces also prefer limbs. Alternatively, distributed responses to faces and limbs may be decorrelated, suggesting that the degree to which a voxel prefers faces is uninformative about the degree to which it prefers limbs.

To address these outstanding fundamental issues, we examined the nature of the functional organization of face- and limb-selective activations in human VTC both across category-selective regions as well as outside them. We measured subjects' brain activations in VTC while they viewed objects from six categories (Fig. 1) using high-resolution fMRI with no spatial smoothing, which provides a more accurate spatial measurement of activations. Using a combination of GLM and MVP analyses, we addressed the following questions: (1) Is there one, or more than one, face-selective and limb-selective activation in lateral VTC on the fusiform gyrus and occipito-temporal sulcus? (2) Do a majority of face- and limb-selective voxels overlap? (3) Is this organization consistent across sessions within subjects, as well as between subjects, and relative to retinotopic visual areas? (4) Is this organization reproducible across paradigms (block, event-related), tasks (1-back, categorization), and sessions (same day or five months apart)? (5) What is the relationship between the distributed responses for faces and limbs? (6) Is there differential information about faces and limbs across highly-, weakly, and non-selective voxels?

Materials and methods

Subjects

Seven subjects (2 female, ages 24–39) participated in four experiments on two separate days about 5 months apart. All subjects participated in additional scans in which we acquired a whole brain anatomical volume and performed standard retinotopic mapping (see Sayres and Grill-Spector, 2008). Written consent was obtained from each subject, and the procedures were approved by the Stanford Internal Review Board on Human Subjects Research.

Experiments

We used gray-level images subtending a visual angle of 7.125° from the fovea presented with Psychophysics Toolbox (Brainard, 1997) using code written in MATLAB (The Mathworks, Natick, MA).

Experiment 1, Day 1 and Experiment 3, Day 2: block design, 1-back task

Experiments 1 and 3 were identical, but conducted on separate days on average 5 months apart. Subjects participated in 2–4 runs of this experiment in separate sessions during which they viewed images of faces, limbs, flowers, houses, cars, guitars, and scrambled objects in 12-s blocks (Fig. 1A). Images from each of our categories appeared in variable viewing conditions. Faces, flowers, houses, cars, and guitars were from a database used in our previous studies

Fig. 1. Experimental designs. (A) Experiment 1, Day 1 and Experiment 3, Day 2. Each block lasted 12-s where each image was presented for 750-ms followed by a 250-ms blank. Blocks included gray-level images of faces, limbs, flowers, cars, guitars, houses, scrambled images, or a blank screen with just a fixation cross. Subjects were required to fixate and to detect by button press when an image repeated. (B) Experiment 2, Day 1. Trials lasted 2-s where each image was presented for 1000-ms followed by a 1000-ms blank. Images were faces, limbs, cars, or houses. Subjects were required to fixate and to categorize images with separate button presses. (C) Experiment 4, Day 2. Each block lasted 12-s where each image was presented for 1000-ms followed by a 500-ms blank. Blocks were faces, limbs, flowers, cars, guitars, houses, or scrambled images. Subjects were required to fixate and categorize images with separate button presses.

(Grill-Spector and Kanwisher, 2005; Grill-Spector et al., 2004; Sayres and Grill-Spector, 2008). Limb stimuli included both upper and lower limbs, always included the digits, sometimes included the arms and the legs, and were used in Sayres and Grill-Spector (2008). Each run consisted of 4 blocks of each condition and 6 blank blocks. Subjects performed a 1-back task where they responded by button press when two consecutive images were identical while maintaining fixation. Categories were counterbalanced within each run and images were not repeated across runs.

Experiment 2, Day 1: event-related, categorization task

One concern about interpreting the results of block design experiments is that the blocking generates a context. To determine whether categorical effects are influenced by this factor, subjects participated in an event-related experiment in which they viewed images of faces, limbs, cars, and houses one at a time in a rapid event-related design (Fig. 1B). Each trial lasted 2-s, where an image was presented for 1-s followed by a 1-s blank. Subjects participated in 6–8 runs each containing 156 trials. For each category, 12 images were seen once ('different') and 2 images were repeated 6 times ('same') during a run. 'Different,' 'same,' and blank trials were counterbalanced for the n–1th trial within each run, and the categories were counterbalanced within each of the 'same' and 'different' trials. Images were not repeated across runs. Subjects were instructed to categorize each of the images using a separate button press for each category while maintaining fixation. Only 'different' trials were used for the analyses presented in this study. Comparison of responses to 'same' trials vs. 'different trials' were performed in a separate study examining the effects of repetition on category-selectivity (Weiner et al., 2010).

Experiment 4, Day 2: block design, categorization task

In 6–8 runs of 29, 12-s blocks, subjects viewed intact, gray-level images of faces, limbs, flowers, cars, guitars, and houses (intact block), which alternated with blocks of scrambled images of these categories (Fig. 1C). Each intact block contained 0–2 scrambled images functioning as catch trials that occurred randomly. Half of the intact blocks contained up to eight different object images ('different') and half of the intact blocks contained up to 8 repetitions of the same object image ('same'). Only 'different' blocks were used in the analyses. There was one different block per category per run, and a total of 8 blocks per category with different images across runs. Subjects were instructed to fixate and categorize images by a separate button press. Comparing the activations during this experiment with those from Experiments 1 and 3 allows the examination of whether the task (1-back vs. categorization) qualitatively changes activation patterns to different categories.

Retinotopic mapping

We defined early visual areas using separate retinotopic mapping scans with standard-resolution fMRI (3 mm voxels). All subjects participated in at least two polar angle scans using a rotating checkerboard wedge and two eccentricity scans using an expanding checkerboard ring (see Sayres and Grill-Spector, 2008). We were able to reliably identify areas V1, V2, V3, hV4, V3ab, V7 (IPS-0), VO-1, and VO-2 (Fig. 2).

hMT+

On Day 1, all subjects also participated in a scan aimed to define hMT+. We defined hMT+ as a region in the posterior inferior temporal sulcus (pITS) that responded more strongly to low contrast

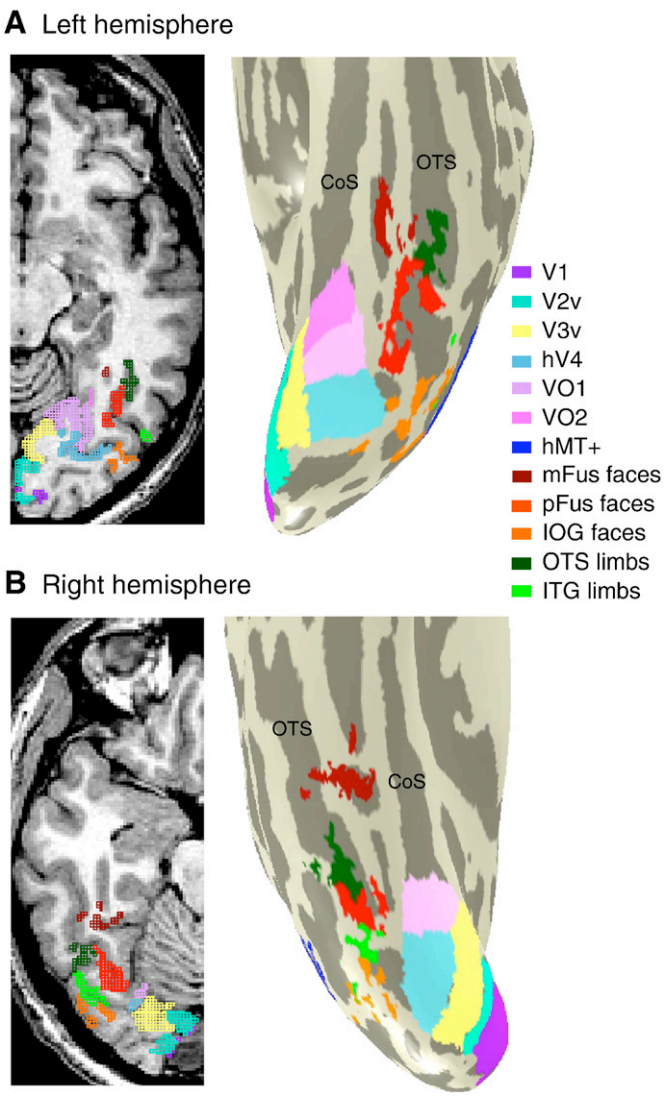

Fig. 2. Visualization of functional ROIs in subject S1. Left: axial slice illustrating the ROIs on the brain volume. Right: same ROIs displayed on the inflated cortical surface. (A) Left hemisphere. (B) Right hemisphere. The right axial slice is 8 mm lower than the left hemisphere to provide axial slices where all ROIs are visible in both hemispheres. See legend for colors of each ROI. pFus: posterior fusiform. mFus: mid-fusiform. OTS: occipito-temporal sulcus. ITG: inferior temporal gyrus; IOG: inferior occipital gyrus. CoS: Collateral sulcus.

expanding and contracting concentric gratings vs. identical stationary gratings (Dumoulin et al., 2000).

fMRI data collection

Scanning

Subjects were scanned on a GE 3-Tesla Signa scanner at the Lucas Imaging Center at Stanford University using a custom-built phased-array, 8-channel surface coil (Nova Medical, Inc. Wilmington, MA, USA).

Experiments 1 and 2, Day 1. We acquired 12 slices at a resolution of $1.5\times1.5\times3$ mm using a two-shot T2*-sensitive spiral acquisition sequence (Glover, 1999) (FOV = 192 mm, TE = 30 ms, TR = 1000 ms, flip angle = 77° and bandwidth = 125 kHz). Inplane anatomicals were acquired with the same prescription using a two-dimensional RF-spoiled GRASS (SPGR) sequence (TE = 1.9 ms, flip angle = 15°, bandwidth = 15.63 kHz).

Experiments 3 and 4, Day 2. We acquired 26 slices at a resolution of $1.5\times1.5\times1.5$ mm using a two-shot T2*-sensitive spiral acquisition sequence (FOV = 192 mm, TE = 30 ms, TR = 2000 ms, flip angle = 77° and bandwidth = 125 kHz). Inplane anatomicals were acquired with the same prescription using a SPGR sequence (TE = 1.9 ms, flip angle = 15°, bandwidth = 15.63 kHz).

Anatomical brain volumes

A high-resolution anatomical volume of the whole brain was acquired with a head coil using a T1-weighted SPGR pulse sequence (TR = 1000 ms, flip angle = 45°, 2 NEX, FOV = 200 mm, resolution of $0.78\times0.78\times1.2$ mm).

Data analysis

Data were analyzed with MATLAB (version 7.3) using the mrVista toolbox (http://white.stanford.edu/software).

Anatomical data

Anatomical volumes were segmented into gray and white matter and from this segmentation we reconstructed the cortical surface for each subject. Each subject's data was aligned to their high-resolution anatomical volume, enabling us to compare regions of interest across scans and to visualize activations on the inflated cortical surface.

Time course processing

Functional data of each session were motion corrected using an affine transformation (Nestares and Heeger, 2000). Time series data were filtered using a temporal high-pass filter with a 1/20 Hz cutoff and then converted to percentage signal change by dividing the time series of each voxel by its mean intensity. Standard general linear model (GLM) analyses were used to create voxel-by-voxel activation maps (Worsley et al., 1997). Data were not spatially smoothed. We estimated the BOLD response amplitudes for each stimulus category by computing the beta coefficients from a GLM applied to the preprocessed time series of each voxel using as predictors the experimental conditions convolved with the hemodynamic impulse response function used in SPM2.

Region of interest (ROI) selection

Functional ROIs. ROIs were defined on a subject-by-subject basis using only Experiment 1, Day 1 data and distinct anatomical and functional boundaries (Fig. 2 shows an example subject). Three face-selective clusters were defined with a contrast of faces > flowers, cars, guitars, and houses ($t>3$, $p<0.002$, voxel level): (1) middle fusiform, mFus (7/7 subjects), (2) posterior fusiform, pFus (6/7), and (3) inferior occipital gyrus, IOG (7/7). Two limb-selective clusters were defined with a contrast of limbs > flowers, cars, guitars, and houses, ($t>3$, $p<0.002$, voxel level): (1) occipito-temporal sulcus, OTS (7/7), extending to the lateral fusiform gyrus and (2) inferotemporal gyrus, ITG (7/7). We also localized a house-selective cluster (houses > faces, limbs, flowers, cars, guitars, $t>3$, $p<0.002$, voxel level) in all subjects along the collateral sulcus (CoS) and parahippocampal gyrus. The house-selective CoS is likely to be similar to a building-selective region that has previously been reported (Aguirre et al., 1998; Epstein and Kanwisher, 1998).

Anatomical ROIs. We also defined four anatomical ROIs on the gray matter (Fig. 3) of each subject and hemisphere to provide an independent and unbiased way to select voxels for our multivoxel pattern (MVP) and titration analyses. The first ROI covered the OTS, fusiform gyrus (FG), and CoS. The posterior edge of this ROI was the anterior boundary of hV4 and the anterior edge of this ROI was the middle of the FG (along the anterior–posterior axis) and is referred to as *whole VTC*. The second and third ROIs were created by dividing the whole VTC ROI down the anterior–posterior axis along the mid-fusiform sulcus to generate lateral (*lateral VTC*) and medial (*medial*

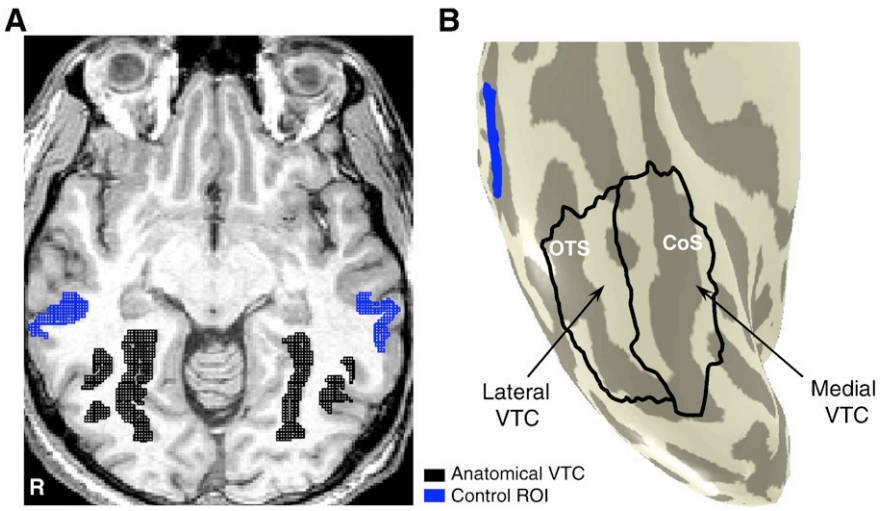

Fig. 3. Location of the control and anatomical ROIs in subject S6. The control ROI (blue) is located on the anterior aspect of the inferior temporal sulcus relative to the anatomical ventral temporal cortex (VTC) ROI (black). (A) Example axial slice on the volume illustrating the relative locations of each ROI in both hemispheres. (B) Inflated cortical surface of the right hemisphere illustrating the same ROIs, as well as the division of the anatomical VTC into lateral and medial partitions along the mid-fusiform sulcus. OTS: occipito-temporal sulcus. CoS: Collateral sulcus.

VTC) partitions. The fourth ROI was a *control ROI* centered on the anterior aspect of the inferior temporal sulcus that extended to the superior temporal sulcus laterally and OTS medially. This ROI falls outside visually-responsive regions and was used to determine whether spurious correlations in the gray matter can yield similar results to our VTC data.

Titration analysis: volume of face, limb, and overlapping voxels

Using the data from Experiment 1, Day 1 and Experiment 3, Day 2, we calculated the overall volume of activated voxels independent of clustering for each of the face or limb-selective contrasts, as well as the overlap between the two as a function of threshold ($3<t$-value <6) in each subject's whole VTC (Fig. 4B). We then converted these values into a proportion by dividing the number of overlapping voxels by the number of face- and limb-selective voxels, respectively (Fig. 4C).

Time series signal-to-noise (tSNR) analyses

To examine whether patchy activations were due to lower signal-to-noise outside than inside activation clusters, we calculated the time series signal-to-noise ratio (tSNR; Kruger and Glover, 2001) in each of Experiments 1 and 3. We created disk ROIs with a 5 mm radius in four locations bilaterally (see Fig. 5A for the disk locations in an example subject). Two of these disks were centered on our face-selective activations, one on the mFus and the other on the pFus. The third disk was centered on the medial VTC along the CoS, and the fourth disk was centered between the two face-selective activations. Within these disks, we extracted the mean raw time series across voxels for each experimental run and computed the tSNR for each experimental run as:

$$tSNR = \frac{mean(timeseries)}{std(timeseries)}.$$

ROI analyses of selectivity

Using each category-selective ROI defined from Experiment 1, Day 1, we examined the magnitude of responses (Fig. 6) and selectivity (Fig. 7) in the other experiments and sessions. Selectivity (d') was calculated separately for each subject using the formula:

$$Selectivity\ (d') = \frac{Preferred\,Amplitude - Nonpreferred\,Amplitude}{\sigma};$$

$$\sigma^2 = \frac{residual\,variance\,from\,GLM}{df}$$

where *Preferred amplitude* is the mean response to the preferred category in each face- or limb-selective ROI. In Fig. 7A, *nonpreferred amplitude* represents the mean response of all other categories. In Fig. 7B, *nonpreferred amplitude* is the mean response of inanimate categories used in all experiments (cars and houses), and we calculated the index twice in each ROI, once relative to faces and once relative to limbs to compare the selectivity of the preferred category to that of the second-best category.

Multivoxel pattern (MVP) analyses across paradigms, tasks, and days

The MVP for each category was represented as a vector of length n (where n is the number of voxels in the ROI) and represents the spatial activation profile for each category. For each voxel we calculated the amplitude (GLM beta) for each condition relative to the mean beta and divided this by the square root of the residual variance of the voxel GLM to convert data into z-scores and remove between-voxels effects. We visualized activations by projecting MVPs of the first layer of gray matter on the cortical surface (Fig. 8).

In order to examine the reliability of the MVPs within a category (i.e. faces in Experiment 1 to faces in Experiment 2, etc.), as well as the relationship of the MVPs between faces and limbs, we measured the correlation between each category within the same session and then across sessions in both our functional, as well as our anatomical ROIs separately in each subject. Fig. 9A represents these correlations averaged across subjects between Experiment 1 and Experiment 2 in the whole VTC, as well as lateral and medial partitions of this ROI. Since the lateral VTC contains voxels with a range of preference to faces and limbs (from strong preference in functional ROIs to weak preference in voxels outside these ROIs), whereas the medial VTC contains voxels that are not selective for either of these categories, we further examined this relationship in the highly-selective voxels for faces and limbs in lateral VTC (i.e. equivalent to the union of our functional ROIs), the weakly-selective voxels in lateral VTC (i.e. the anatomical lateral VTC ROI excluding our functional ROIs), and the non-selective voxels in medial VTC (i.e. the anatomical medial VTC ROI also excluding house-selective voxels; Fig. 9B). To test the stability of our results across days and experiments, we calculated correlations between Experiments 3 and 4 using the Day 2 data and the same VTC partitions from Experiment 1, Day 1 (Fig. 9C). We also ran these analyses in the control ROIs to empirically estimate the baseline correlation between MVPs in gray matter. An analysis of MVPs across all categories in the control ROI show that the average within- and between-category

correlations were not significantly different than zero indicating that zero correlation is an appropriate baseline. Thus, we tested the significance of MVP correlations compared to zero. All statistical tests on correlations were conducted after performing a Fisher's transformation on the resulting within- and between-category correlations.

We assessed the stability of MVPs, as well as the amount of information in the distributed responses, by applying a winner-take-all (WTA) classifier. For each subject, we performed this analysis with Experiment 1, Day 1 as the training set and the three other independent experiments as testing sets and then again using the Experiment 3, Day 2 data as the training set and the remaining three experiments as testing sets. The WTA determines the category based on the highest correlation between the training and testing set. We report in Fig. 10 the mean classification accuracy across all categories and training sets. Chance performance is 16.7% because each category's MVP is compared to six category MVPs. In Fig. 11, we show the classification performance separately for different stimuli. Here we averaged the classifier performance for guitars, cars, and flowers to illustrate the average classification for objects.

Results

Consistent spatial relationship of face- and limb-selective activations relative to each other as well as retinotopic regions

We examined the spatial characteristics of face- and limb-selective activations without spatial smoothing in Experiment 1 to test if there is consistent spatial organization of face- and limb-selective regions in ventral occipital-temporal cortex. Using GLM contrasts and retinotopy, we determined the spatial organization of face- and limb-selective activations relative to each other, as well as relative to retinotopic areas as previous studies reported face-selective activations lateral to hV4 (Brewer et al., 2005; Halgren et al., 1999) and VO-1/2 (Arcaro et al., 2009; Brewer et al., 2005). Fig. 2 illustrates this organization on the brain volume and Fig. 4A on the inflated cortical surface. We located three face-selective regions in both hemispheres using a statistical contrast of faces>flowers, cars, guitars, and houses, ($t>3$, $p<0.002$, voxel level). Each cluster had separate anatomical locations where the first is most often located on the mid-fusiform sulcus (mFus) sometimes extending laterally onto the occipito-temporal sulcus (OTS), the second on the posterior fusiform gyrus (pFus) sometimes extending into the OTS/inferior temporal gyrus (ITG), and the third on the inferior occipital gyrus (IOG). Prior studies have typically combined the mFus and pFus together to form the traditional fusiform face area (e.g. Grill-Spector et al., 2004) or have attempted to divide them into separate FFA clusters (e.g. FFA-1/2; Pinsk et al. 2009).

We located two limb-selective regions bilaterally using a statistical contrast of limbs>flowers, cars, guitars, and houses, ($t>3$, $p<0.002$, voxel level). Both of these clusters had independent locations where the more anterior cluster most often overlapped with the OTS and sometimes extended into the lateral FG, and the other was found most typically on the ITG (Figs. 2 and 4A). The former likely corresponds to the FBA (or FBA-1/2; Pinsk et al., 2009) and the latter has been included in some studies as an inferior portion of the extrastriate body area (EBA; Peelen and Downing, 2005, 2007a,b; Spiridon et al., 2006). We separated the ITG activation from the other limb-selective clusters around hMT+ because they are consistently separated by a region with differing functional selectivity, namely hMT+ (see Supplementary data and Supplemental Fig. 1).

Each face-selective cluster has distinct boundaries from the others that would otherwise be missed without examining their relation to the limb-selective activations, hV4, VO-1/2, and hMT+ (Fig. 4A). Specifically, the face-selective mFus has two distinct boundaries: (1) anterior and medial to the limb-selective OTS and (2) anterior and lateral to VO-1/2. Face-selective pFus has three boundaries: (1) posterior and medial to limb-selective OTS, (2) anterior and lateral to hV4, and (3) anterior and inferior to limb-selective ITG. The IOG has two boundaries: (1) posterior to limb-selective ITG and (2) lateral to hV4. Likewise, the face-selective activations serve as reliable boundaries for separating the limb-selective activations. In particular, the limb-selective OTS splits the two fusiform face activations, where it is posterior and lateral to face-selective mFus and also anterior and lateral to face-selective pFus. Comparatively, the limb-selective ITG has four boundaries: (1) lateral to hV4, (2) posterior and lateral to face-selective pFus, (3) anterior to face-selective IOG, and (4) inferior and partially overlapping hMT+. The location of this activation is more variable compared to the limb-selective OTS activation, but it is consistently inferior to hMT+ (Fig. 4A, Supplemental Fig. 1 and Supplementary data). Consequently, our data show that face- and limb-selective regions have consistent locations both relative to each other, as well as relative to retinotopic regions and hMT+.

Minimal overlap between face- and limb-selective voxels

Using an independent VTC anatomical ROI encompassing the OTS, FG, and CoS (see Materials and methods, and Fig. 3), we quantified the volume of face- and limb-selective activations relative to their overlap in both sessions using the same experiment (Experiment 1 on Day 1 and Experiment 3 on Day 2). We found significantly more face than limb-selective voxels in VTC ($Fs_{1,84}>12.9$; $ps<10^{-4}$), significantly more face or limb activation compared to overlapping voxels independent of threshold ($Fs_{1,84}>6.7$; $ps<0.01$, Fig. 4B illustrating the Experiment 1, Day 1 data) and no effect of hemisphere ($F_{1,288}=0.11$, $p=.74$). For example, with a threshold of $t=4$, there was on average 558 mm^3 of face activation, 210 mm^3 of limb activation, and 66 mm^3 of overlap across subjects and hemispheres (Fig. 4B). These effects are replicated in Experiment 3, Day 2 with a higher resolution of 1.5 mm isotropic voxels (more face than limb voxels: $Fs_{1,84}>10.3$; $ps<0.002$; more face or limb activation compared to overlapping voxels: $Fs_{1,84}>6.1$; $ps<0.02$; no effect of hemisphere: $F_{1,288}=0.89$, $p=.35$). Since there is no effect of hemisphere, we quantified the amount of overlap as a proportion of overlapping voxels relative to face- and limb-selective voxels across both hemispheres. This analysis indicates that in either session less than 28% of the limb-selective voxels in VTC also respond selectively to faces, and less than 13% of face-selective voxels also respond selectively to limbs (Fig. 4C). A 2-way ANOVA using as factors category (proportion overlap for faces and limbs across thresholds) and session (Day 1/Day 2), illustrates a main effect of category ($F_{1,189}=28.0$; $p<10^{-5}$) and no main effect of session ($F_{1,189}=1.64$; $p=.20$), indicating that there is less overlap for faces compared to limbs and these proportions are consistent across sessions and variations in resolutions. Thus, there is a consistent spatial organization of face- and limb-selective activations that minimally overlap with each other as measured by high-resolution scanning methods and no spatial smoothing.

The patchy organization is not due to lower signal-to-noise in high-resolution fMRI

High-resolution fMRI measurements of face- and limb-selective activations are patchier than activations measured with standard-resolution fMRI (voxels of 3 mm on a side, or larger). One concern is that the patchiness results from lower signals or lower time series signal-to-noise (tSNR) in high-resolution fMRI measurements compared to standard-resolution measurements. To examine these possibilities, we examined the mean signal levels and tSNR within and between our clusters of activations. First, we found no evidence for signal drop out between face- or limb-selective clusters (Fig. 5A). Signal drop out typically occurred anterior to our VTC region due to susceptibility artifacts in the region behind the ear canals (anterior to the white disk ROI in Fig. 5A) and in some instances lateral to hV4. Second, the tSNR (see Materials and methods) was comparable within and outside 5 mm disks centered on the mFus and pFus patches

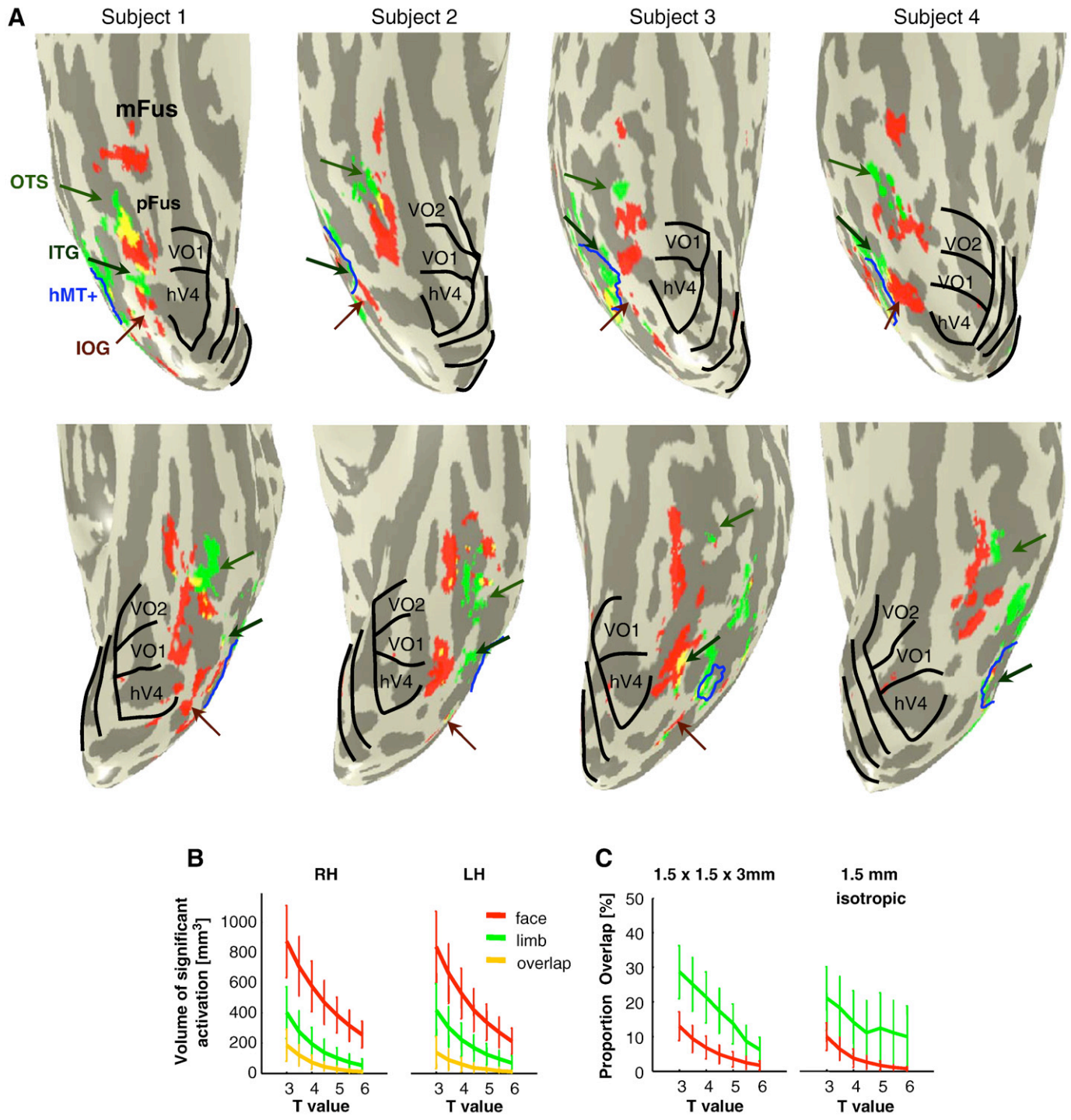

Fig. 4. Face- and limb-selective activations in ventral temporal cortex (VTC): consistent spatial relationship and minimal overlap. (A) GLM contrasts from Experiment 1, Day 1 indicating nonoverlapping faces vs. objects (cars, houses, flowers and guitars, $t>3$, voxel level, red), nonoverlapping limbs vs. objects ($t>3$, green), and overlapping (yellow) activations on the inflated cortical surface of four subjects zoomed on the fusiform gyrus. Visual areas V1-hV4, as well as VO-1 and VO-2, are outlined in black and were defined from retinotopy scans. hMT+ is outlined in blue and was defined from a separate localizer scan. Light green arrows indicate the location of the limb-selective OTS, dark green arrows indicate the location of the limb-selective ITG, and dark red arrows indicate the location of the face-selective IOG. Top: right hemisphere; bottom: left hemisphere. (B) Volume of VTC face- (red) and limb-selective (green) activation and overlap (yellow) as a function of threshold-value separately for each hemisphere from Experiment 1, Day 1. A value of $t=3$ is significant at $p<0.002$, and $t=6$ is significant at $p<10^{-8}$. Error bars: SEMs across subjects. (C) Proportion of the number of overlapping voxels compared to the number of limb-selective (green) and face-selective (red) voxels across both hemispheres in Experiment 1, Day 1 ($1.5\times1.5\times3$ mm) and Experiment 3, Day 2 (1.5 mm isotropic). pFus: posterior fusiform. mFus: middle fusiform. OTS: occipito-temporal sulcus. ITG: inferior temporal gyrus; IOG: inferior occipital gyrus.

(Fig. 5B). A 2-way analysis of variance (ANOVA) on the tSNR values across disks and experiments showed no effect of disk location ($F_{3,48}=0.60$; $p=.62$), experiment ($F_{1,48}=0.01$; $p=.92$), or interaction ($F_{3,48}=0.08$; $p=.97$). Thus, our smaller, nonoverlapping face- and limb-selective activations are not a result of signal drop out or low tSNR values for either experiment.

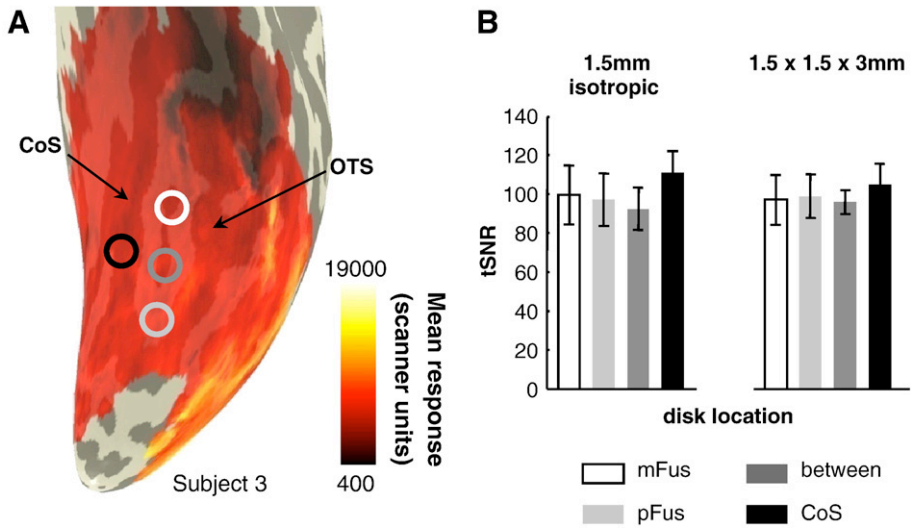

Fig. 5. tSNR measurements: patchiness is not due to signal drop out. (A) Mean map illustrating the extent of activation in raw scanner units on the inflated cortical surface of an example subject's right hemisphere zoomed on the fusiform gyrus. The map is depicted semi-transparently to allow the viewing of the underlying anatomy. Colored disks illustrate the location of the four disk ROIs. Disks were centered on our face-selective activations (mFus and pFus), between these activations, and on the CoS. (B) tSNR measurements from these disks ROIs averaged across hemispheres and subjects. Left: 1.5 mm isotropic measurements from Day 2 session. Right: 1.5×1.5×3 mm measurements from Day 1 session. Error bars: SEMs across subjects. OTS: occipito-temporal sulcus; CoS: collateral sulcus.

Reproducible profile of time series and selectivity across scanning sessions

We next examined the selectivity of responses and the stability of category-selectivity within each of our five functional ROIs. These ROIs were defined from Experiment 1, Day 1 data and we measured responses and selectivity by extracting the time series from these ROIs in each of the three other independent experiments. We did not exclude the overlapping regions. While there are differences in the absolute magnitude of response across experiments, which is expected as signals in event-related experiments (Experiment 2) are lower than block experiments (Experiment 3, 4), the relative profile of response to different objects in an ROI is preserved. As illustrated in Fig. 6, face-selective IOG, pFus, and mFus all illustrate the highest percentage signal amplitude for faces across experiments, while limb-selective ITG and OTS illustrate the highest percentage signal for limbs across experiments. Similarly, the ranking of nonpreferred stimuli is consistent. For example, in face-selective mFus, houses consistently yielded the lowest response, cars yielded a higher response, and limbs yielded the second-highest response.

To quantify the amount of selectivity within each region, we calculated d' values for each region relative to all categories across experiments (see Materials and methods; Fig. 7A) and found differential selectivity across ROIs. First, each face- and limb-selective cluster has a d' greater than 0, indicating significant selectivity compared to all the other categories ($ts>3.6$, $ps<.006$). Second, there is a difference in selectivity across face-selective clusters (main effect of region, $F_{2,51}=3.43$, $p<.04$), where the mFus has higher face selectivity than the IOG ($t(20)=4.09$, $p<10^{-5}$), but the selectivity of pFus is not significantly different than either cluster ($ts<1.68$, $ps>.10$). Third, there is a reverse trend in the limb-selective clusters, where the posterior ITG illustrates significantly more limb selectivity than the more anterior OTS ($t(20)=5.9$, $p<10^{-6}$).

We next calculated d' values for the best and second-best category in each region relative to the overlapping categories across experiments (cars and houses, Fig. 7B). The selectivity indices for faces in limb-selective clusters, and the selectivity for limbs in face-selective mFus and IOG are significantly above 0 ($ts>3.52$, $ps<.01$), illustrating that a category-selective region can demonstrate selectivity for additional categories. Selectivity indices for limbs in both limb-selective clusters were significantly higher than the selectivity indices for the second-best category, faces ($ts>8.03$, $ps<10^{-4}$). Similarly, selectivity indices for faces in face-selective pFus and mFus were significantly higher than the selectivity indices for the second-best category, limbs ($ts>5.2$, $ps<.002$). However, the face-selective IOG had similar selectivity to faces and limbs as compared to houses and cars ($t(6)=.05$, $p=.96$) despite the fact that this region was defined based on its selectivity to faces vs. objects (Fig. 7B). The higher response for limbs in the IOG compared to the mFus and pFus is partially due to a larger degree of overlap between face- and limb-selective activations on the lateral surface. We found that 30% of the face-selective voxels in the IOG overlap with limb-selective voxels, and this overlap is significantly larger ($ps<.03$) compared to the 7% and 5% overlap in the pFus and mFus, respectively. When we excluded voxels from the IOG that were significantly limb-selective and re-calculated d' we found that limb selectivity significantly decreased from 1.14 to .91 ($p<0.02$) and there was a slight preference for faces. These results raise the question of whether this IOG region should be labeled as 'face-selective' as commonly done in prior studies (Gauthier et al., 2000; Haxby et al., 2000; Grill-Spector et al., 2004, Pinsk et al., 2009) and suggest that caution should be exerted when defining a region as 'selective to a category' when a small number of stimuli are used as a comparison.

Taken together, GLM analyses illustrate that activations for limbs and faces alternate in a series of complementary and largely nonoverlapping bands along a posterior–anterior axis across the ITG and OTS for limbs and across the IOG and FG for faces. Limb-selective activations are consistently lateral to the face-selective activations and positioned more posteriorly, creating a series of alternating clusters that are shifted on both a lateral/medial axis as well as an anterior/posterior axis. These face- and limb-selective clusters have distinct selectivities and are arranged in a consistent organization relative to each other and relative to retinotopic visual areas. Therefore, we label these face- and limb-selective activations according to their anatomical location and categorical preference because (1) the activations fall in different anatomical locations (Figs. 2 and 4A), (2) there is typically at least one cluster with a different category preference in between them with little overlap (Figs. 2 and 4), and (3) there is differential face and limb selectivity across clusters which is consistent across experiments (Figs. 6 and 7).

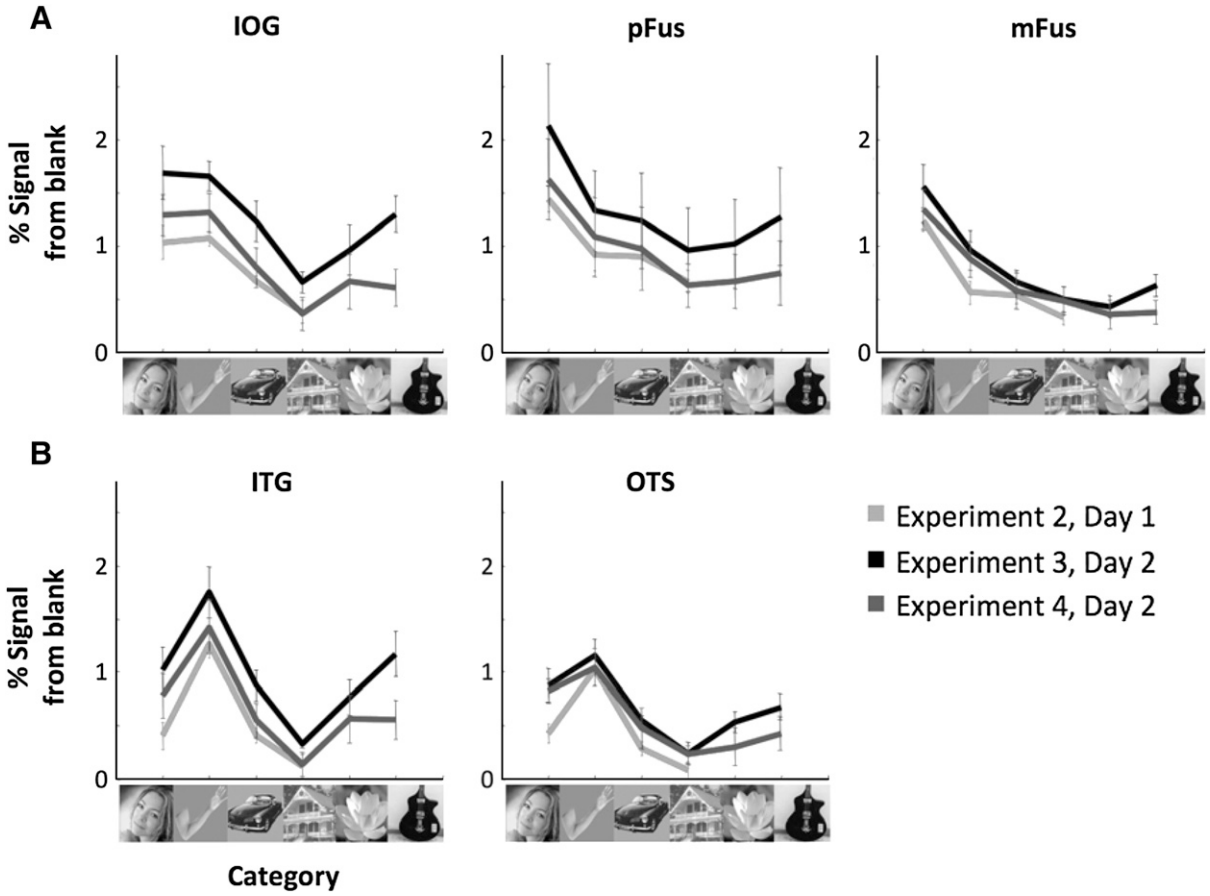

Fig. 6. Stable response amplitudes to object categories across experiments. ROIs were defined from Experiment 1, Day 1. Response amplitudes were extracted from the remaining three sessions for each ROI and were averaged across subjects. (A) Face-selective regions: IOG, pFus, and mFus (from left to right). (B) Limb-selective regions: ITG and OTS (from left to right). Error bars indicate SEMs across subjects. See legend for color indexing. Experiment 2, Day 1 only contains four categories, while the other two experiments contain six.

Multivoxel patterns (MVP) between faces and limbs are anticorrelated in highly- and weakly-selective voxels in lateral VTC

We complemented the GLM analyses with multivoxel pattern (MVP) analyses with the following goals: (1) to examine the MVPs to object categories across the entire VTC without thresholding, (2) to determine the relationship between spatially distributed responses to faces and limbs across the entire VTC within and outside category-selective regions, and (3) to evaluate the amount of category information present within and outside category-selective regions by measuring classification performance.

Fig. 8 illustrates the MVP of responses to our six object categories in an example subject's brain. Each category shows a different distributed pattern of response across VTC, with faces and limbs showing higher responses than the mean in lateral VTC and houses showing higher responses than the mean in medial VTC. Cars and flowers show a more diffuse activation. Two effects are notable from visually inspecting the patterns. First, limbs and houses, as well as faces and guitars, show opposite patterns of response, where 'hot spots' (warm colors) for one category illustrate 'troughs' (cool colors) for the opposing category. Second, the hot spots for faces and limbs alternate. That is, even in unthresholded MVPs it is apparent that different voxels in VTC show preferential responses to faces and limbs.

To quantify the reproducibility and relationship between face and limb distributed responses, we calculated the correlation between face and limb MVPs across the whole VTC anatomical ROIs in Experiment 1 and Experiment 2 on Day 1. We found highly positive within-category correlations for faces and limbs indicating that these patterns are reproducible across Experiments 1 and 2 ($ts > 10.6$, $ps < 10^{-5}$; Fig. 9A) independent of task and experimental paradigm.

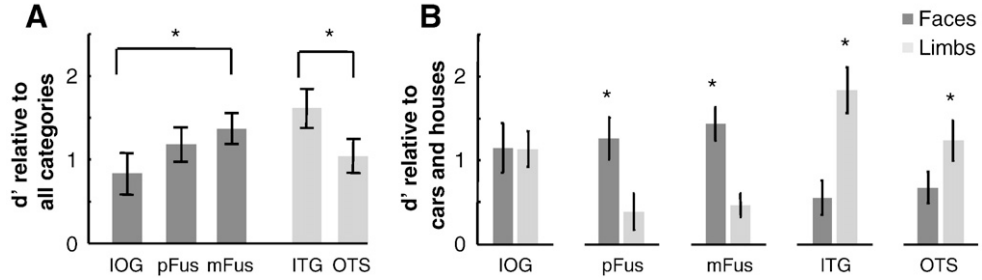

Fig. 7. Differences in selectivity across regions. Selectivity indices (d') averaged across independent sessions and subjects. (A) Selectivity for the preferred category in each category-selective cluster. Asterisks: significant difference in selectivity between ROIs ($p < 10^{-5}$). (B) Selectivity measured separately for the top two categories in each ROI relative to the two overlapping object categories across all experiments (cars and houses). Asterisks: significant difference in face- and limb selectivity ($p < .002$).

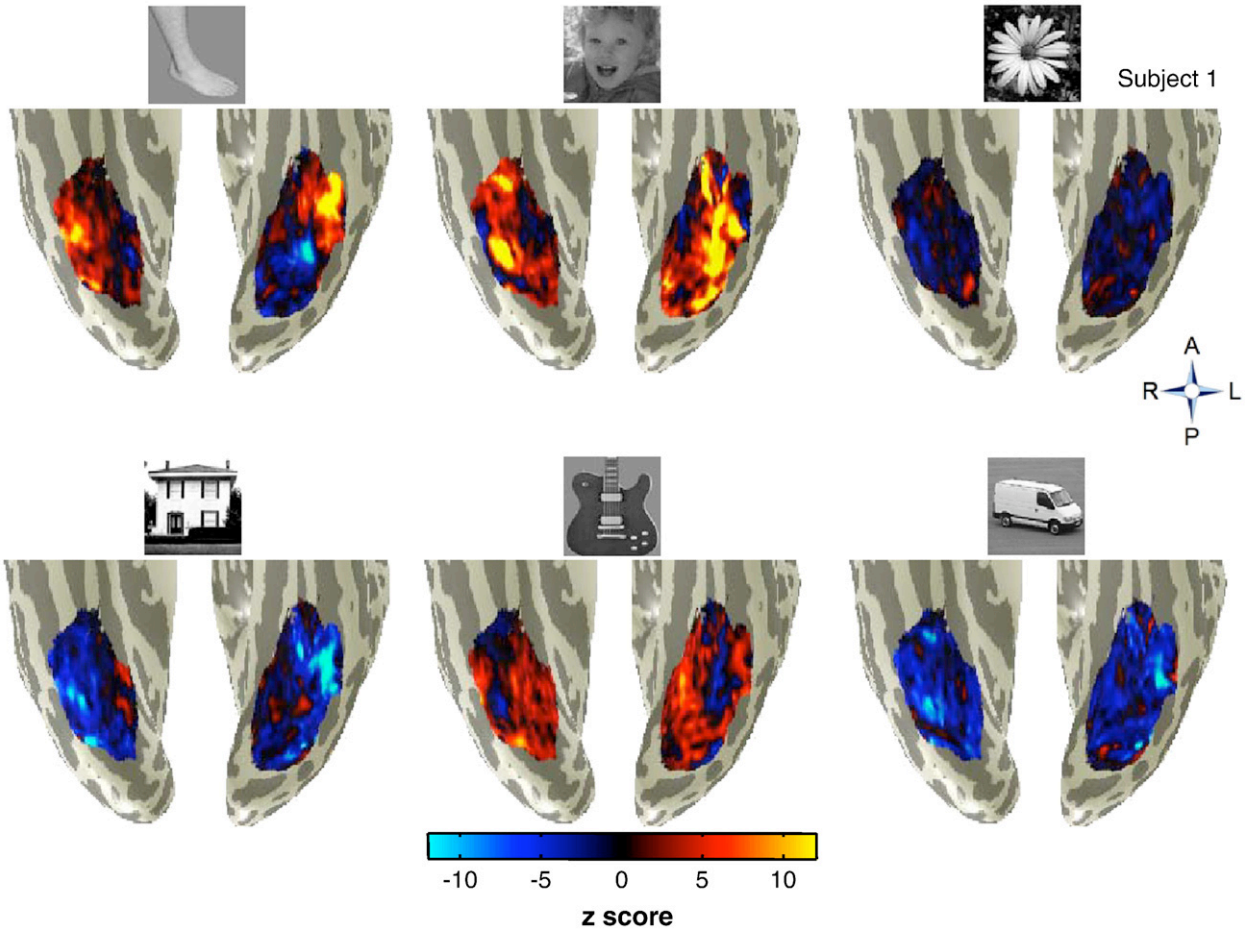

Fig. 8. Multivoxel patterns (MVP) of object categories in ventral temporal cortex (VTC). MVP responses of object categories across the anatomical VTC are shown as normalized z-score values projected on the inflated cortical surface of subject S1 using Experiment 1, Day 1 data. Warm colors illustrate z-score values higher than the mean response across all categories, while cool colors represent z-score values lower than the mean response across all categories.

Notably, the between-category correlations between face and limb MVPs are significantly negative ($t(6) = 3.7$, $p < .005$), indicative of anticorrelated responses across the whole VTC. We asked whether this anticorrelated response pattern is driven by voxels from category-selective ROIs or from the non-selective voxels outside these ROIs. Thus, we divided the VTC along the mid-fusiform sulcus to create a lateral VTC ROI that includes the alternating face and limb clusters and a medial VTC ROI that excludes this structure (Fig. 3). We find (1) significantly greater anticorrelation between face and limb MVPs in lateral compared to either whole or medial VTC ($ts > 25.6$, $ps < 10^{-7}$) and (2) higher within-category correlation in lateral VTC compared to both whole and medial VTC ($ts > 4.47$, $ps < .004$, Fig. 9A). This indicates that distinct MVPs for faces and limbs are driven by separate activation patterns to these categories in lateral VTC, and not from the low responses to these categories in medial VTC.

We next determined whether the relationship between face and limb activation patterns is different across highly-, weakly-, and non-selective voxels. Thus, we repeated the MVP analyses within (1) the union of our face- and limb-selective ROIs in lateral VTC that we refer to as *highly-selective voxels*, (2) the voxels in lateral VTC excluding the highly-selective voxels that we refer to as *weakly-selective*, and (3) the voxels in medial VTC that are not face-selective, limb-selective or house-selective, which we refer to as *non-selective* (see Materials and methods). Notably, MVPs for faces and limbs are more reproducible across the highly-selective voxels compared to the weakly- or non-selective voxels (main effect of region; $F_{2,36} = 61.5$, $p < 10^{-5}$), and are more distinct (anticorrelated) compared to weakly-selective or non-selective voxels (Fig. 9B, main effect of region; $F_{2,18} = 18.5$, $p < 10^{-5}$). Interestingly, even though non-selective voxels in medial VTC contain no face- or limb-selective voxels, the MVPs for faces and limbs are reproducible as there are significantly positive within-category correlations for these categories ($ts > 3.35$, $ps < .008$). However, the between-category correlation is not significantly different than zero ($t(6) = .70$, $p = .51$), indicating that the MVPs for faces and limbs are functionally independent in medial VTC. We examined the reproducibility of these results by using the same ROIs from the Day 1 session and extracting MVPs from Experiments 3 and 4 from the Day 2 session using 1.5 mm isotropic voxels. We replicate our results from the previous analysis, finding the same relationship among MVPs in the different VTC partitions (Fig. 9C, main effect of region; all $F_{2,18} > 6.6$, $ps < 10^{-3}$). Therefore, the anticorrelation between face and limb MVPs is (1) not driven by non-selective voxels and (2) not limited to highly-selective voxels, but also extends to weakly-selective voxels in lateral VTC.

Finally, to examine if this decorrelated relationship is restricted to non-selective voxels, we repeated our MVP analyses separately in the mFus, pFus, and IOG functional ROIs defined from Experiment 1, Day 1 data (Fig. 4) and examined the correlation between face and limb MVPs using the Day 2 data (Supplemental Fig. 2). We found significant within-category correlations for both faces and limbs in each of the ROIs (all $ts > 4.05$, all $ps < .005$). However, the between-category correlation of face and limb MVPs were not significantly different than zero in any of the ROIs (all $ts < 1.09$, all $ps > .32$). Thus, there is a different relationship between distributed responses for faces and limbs within functional ROIs compared to across ROIs, where MVPs are functionally independent within an ROI and

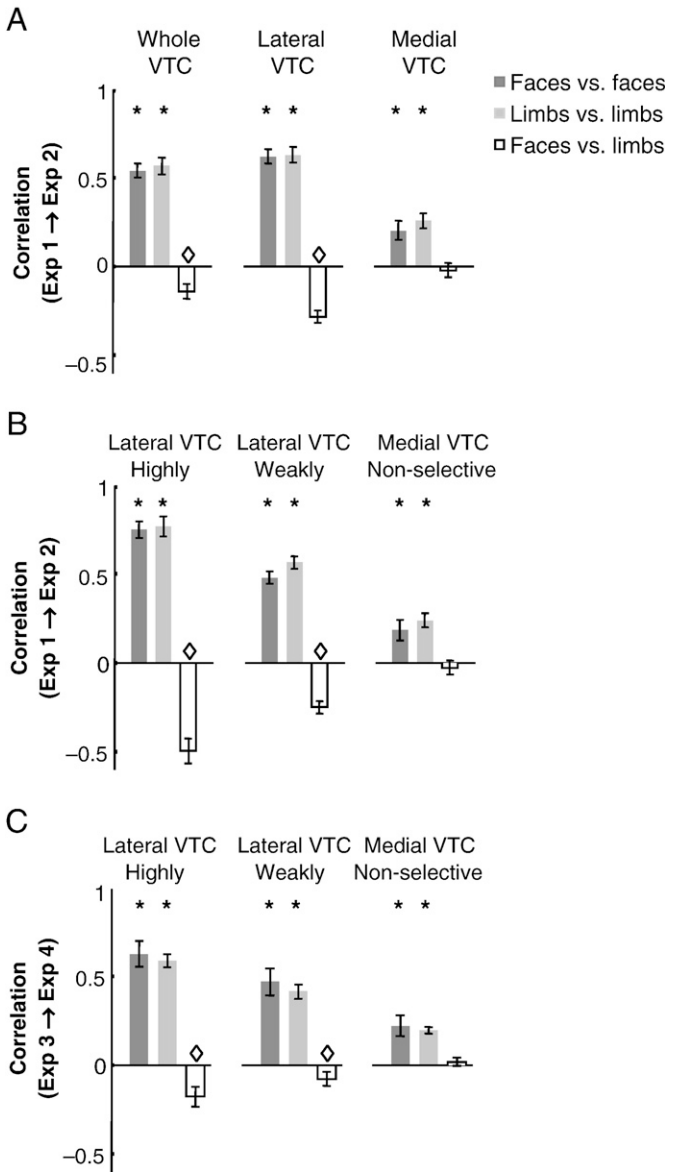

Fig. 9. Reproducibility of face and limb MVPs: patterns are anticorrelated in highly- and weakly-selective voxels in lateral VTC, but decorrelated in medial VTC. (A) Within- and between-category correlations of face and limb MVPs. Correlations were calculated across Experiments 1 and 2 in Day 1 in the whole (left), lateral (middle), and medial VTC (right). (B) Within- and between-category correlations between face and limb MVPs across Experiments 1 and 2 in Day 1. Correlations were calculated separately within highly-, weakly-, and non-selective voxels. Highly-selective voxels are the union of face- and limb-selective voxels in lateral VTC which are significant ($p<0.002$) for the GLM contrast illustrated in Fig. 4 in lateral VTC. Weakly-selective voxels are voxels in lateral VTC excluding the highly-selective voxels. Non-selective voxels are medial VTC voxels excluding face-, limb-, or house-selective voxels. (C) Within- and between-category correlations between face and limb MVPs using the same ROIs as in (B), but for Experiments 3 and 4 in Day 2 session. Left: highly-selective; Middle: weakly-selective; Right: non-selective. Error bars: SEMs across subjects. Asterisks: within-category correlations that are significantly higher than zero ($p<.008$). Diamonds: between-category correlations that are significantly less than zero ($p<.04$).

anticorrelated across ROIs. Interestingly, the IOG shows similar within-category correlations for faces and limbs ($t(6)=1.27$, $p=.25$), the pFus has a trend for more positive within-category correlation for faces than limbs ($t(5)=2.47$, $p=.056$), and the mFus reveals significantly higher within-category correlations for faces than limbs ($t(6)=4.44$, $p<.004$; Supplemental Fig. 2). These results further support a gradient of face processing across these ROIs as suggested previously by our selectivity analyses.

Taken together, our results across sessions indicate that the MVPs for faces and limbs are anticorrelated when using the entire VTC (Fig. 9A) and this anticorrelation is driven by separate subsets of voxels in lateral VTC that are highly- or weakly-selective to either faces or limbs (Figs. 9B–C). That is, there are distinct subsets of voxels outside the category-selective ROIs that have opposite preferences to faces and limbs. However, this relationship does not extend to voxels within functionally selective ROIs or non-selective voxels because these voxels have independent information, where the degree to which a voxel responds to a face does not predict its response to limbs (and vice versa).

Lateral VTC contains more information about faces than medial VTC

We next assessed the amount of category information within MVPs across VTC voxels compared to MVPs within the control ROI and V1 by applying a winner-take-all (WTA) classifier on these MVPs. We used either Experiment 1, Day 1 data as the training set, or Experiment 3, Day 2 as the training set, and each of the other experiments as testing sets (see Materials and methods). A WTA classifier trained with the whole VTC data determines the object category from the MVPs well above the 17% chance level (mean accuracy ± SEM: 78% ± 3%, $ps<10^{-5}$, Fig. 10, right bar). Classification performance was similar across experiments and training sets. A 2-way ANOVA using as factors training set and testing experiment revealed no effects of training set ($F_{1,36}=3.1$, $p=.09$), experiment ($F_{2,36}=1.5$, $p=.23$), or interaction ($F_{2,36}=1.9$, $p=.17$). Similar classification accuracy was found when applying the classifier to either lateral or medial VTC data alone (Fig. 10, middle bars). Further, the classifier's performance is not a result of spurious correlations within gray matter because the WTA's classification performance in a control gray matter ROI is not significantly different than chance (Fig. 10 — left bar). Thus, category information in MVPs is consistent across tasks (categorization, 1-back) and experimental designs (block, rapid event-related) and days.

We next examined if classification performance on VTC data is driven by low-level visual differences between images of different categories by comparing classification performance on VTC data to V1 data. We reasoned that if category effects were driven by low-level differences between stimuli, we would find similar classification performance on V1 data. WTA classification accuracy on V1 data was significantly above chance (mean classification accuracy ± SEM: 45% ± 6%, $t(6)=4.96$, $p<.003$) illustrating that there are low-level differences between images of different categories. However, classification within each of the VTC partitions was significantly higher than V1 classification (all $ts>5.99$, all $ps<10^{-4}$, Bonferroni corrected for multiple comparisons). These results indicate that categorical information of VTC MVPs are not just driven by low-level visual information in our stimuli.

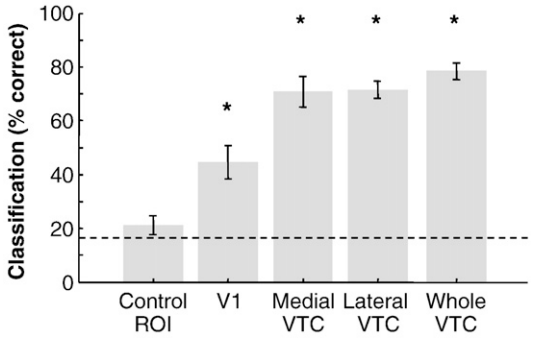

Fig. 10. More category information in distributed responses across VTC than V1 or a control gray matter ROI. Winner-take-all (WTA) classification performance averaged across all subjects, categories, and training sets. Dotted line indicates chance classification performance. Error bars: between subjects SEMs. Asterisks: significantly above chance classification ($p<.001$).

We further assessed the amount of information in different subsets of VTC voxels by applying a WTA classifier separately for the highly-, weakly-, and non-selective voxels. We examined the classification performance separately for faces, limbs, houses, and objects (average classification performance for flowers, guitars, and cars). A WTA classifier trained with either Experiment 1, Day 1 or Experiment 3, Day 2 data and tested with the other experiments determines the category significantly above the 17% chance level for each of these categories and in each of the VTC partitions ($t(6) = 3.44$, $p < .007$; Fig. 11).

Classifier performance was generally highest for faces and lowest for objects (main effect of category, $F_{3,72} = 33.8$, $p < 10^{-5}$). A 2-way ANOVA using as factors region (highly-selective voxels in lateral VTC/weakly-selective voxels in lateral VTC/non-selective voxels in medial VTC) and category (faces/limbs/houses/objects), illustrates that there are different amounts of information in the MVPs of highly-, weakly, and non-selective voxels (category × ROI interaction $F_{6,72} = 6.2$, $p < 10^{-5}$). In particular, face classification is best for both the highly- and weakly-selective voxels in lateral VTC. However, there is significantly less information for faces in medial VTC. Classification performance for faces is 66% in medial VTC, compared to the highly- and weakly-selective voxels in lateral VTC where classification performance is near perfect at 97% and 100%, respectively ($ts > 4.77$, $ps < .003$; Fig. 11). In addition, classification for houses shows an opposite trend where classification performance using non-selective voxels in medial VTC is slightly higher compared to its performance using the highly-selective face- and limb-selective voxels in lateral VTC ($t(6) = 2.1$, $p < 0.08$). For limbs, we find similar classification performance across the different VTC subdivisions with an average classification of 94%, 91%, and 83% in highly-, weakly-, and non-selective voxels, respectively. In sum, our classifier analyses illustrate that there are differential amounts of distributed information for faces, but not limbs, in voxels that are highly-, weakly-, or non-selective for these categories.

Discussion

Using high-resolution fMRI (HR-fMRI) paired with general linear model (GLM) and multivoxel pattern (MVP) analyses, we illustrate a series of alternating face- and limb-selective activations that are arranged in a consistent spatial organization relative to each other as well as retinotopic regions and hMT+. These findings resolve an inconsistency in the literature regarding the location and definition of these regions in ventral temporal cortex (VTC). Specifically, our data illustrate that there is not just one distinct region selective for each category (i.e. FFA and FBA) in VTC, but rather a series of face- and limb-selective clusters that minimally overlap, with a consistent organization relative to one another on a posterior to anterior axis on the occipito-temporal sulcus (OTS) and fusiform gyrus (FG). Our results further illustrate that even in weakly-selective voxels outside of these clusters in lateral VTC, the distributed responses for faces and limbs are distinct from one another. Nevertheless, there is significantly more face information in the distributed responses in weakly- and highly-selective voxels in lateral VTC as compared to the non-selective voxels in medial VTC, indicating differential amounts of information in these different subsets of voxels where weakly- and highly-selective voxels are more informative than non-selective voxels. Taken together, our data support a sparsely-distributed organization of face- and limb-selective activations in VTC, whereby sparseness refers to the presence of several face- and limb-selective clusters in VTC with a distinct, minimally overlapping organization and distributed refers to the presence of information in weakly- and non-selective voxels outside of these clusters.

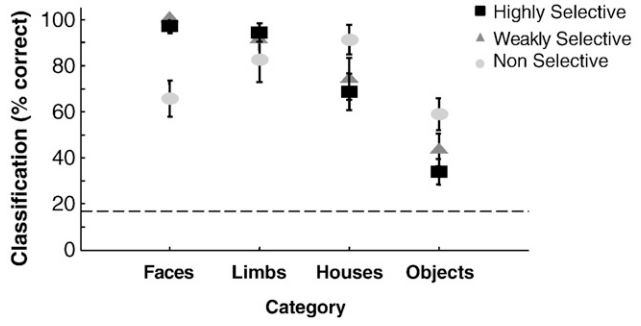

Fig. 11. Significantly more face information in MVP across highly- and weakly-selective voxels in lateral VTC compared to non-selective voxels in medial VTC. Winner-take-all (WTA) classification performance averaged across all subjects, training sets, and sessions. Dotted line indicates chance performance. Error bars indicate between subjects SEMs. All classifier performances were significantly above the 17% change level for all categories ($p < .007$). Classification performance is significantly better for faces in highly- and weakly-selective voxels as compared to non-selective voxels ($p < .003$).

Multiple fusiform face activations are organized in a consistent manner

There is significant variation across studies in the location, number, and definition of face-selective regions in occipito-temporal cortex, as well as no definitive criteria for deciding when a face-selective activation should be considered an area. First, there is a discrepancy in the literature as to where the FFA and OFA are located in VTC. Some groups delineate an anterior fusiform face-selective activation as the FFA and a posterior fusiform activation as the OFA if an activation on the inferior occipital gyrus (the typical location of the OFA) is absent (e.g. Tsao et al., 2008). Other groups merge the two fusiform clusters together as the FFA if the more lateral IOG activation is present (Grill-Spector et al., 2004). Second, high-resolution fMRI (HR-fMRI) indicates that the FFA as measured with standard-resolution fMRI (SR-fMRI) breaks apart and contains clusters that are not face-selective (Grill-Spector et al., 2006). Third, recent SR-fMRI studies indicate that there are more than just three face-selective regions in the occipital and temporal lobes: including two regions on the fusiform gyrus (FFA-1 and FFA-2; Pinsk et al., 2009), a region in anterior temporal cortex 40 mm in front of the more anterior fusiform face-selective activation (Kriegeskorte et al., 2007; Pinsk et al., 2009; Rajimehr et al., 2009; Tsao et al., 2008), and two regions on the anterior and middle STS (Pinsk et al., 2009). Fourth, neuroimaging studies in non-human primates illustrate the same variability in the number of face regions in monkey inferotemporal cortex, varying across studies from 2–6 regions (Hadj-Bouziane et al., 2008; Hoffman et al., 2007; Logothetis et al., 1999; Moeller et al., 2008; Pinsk et al., 2009; Pinsk et al., 2005; Tsao et al., 2003; Tsao et al., 2008). Fifth, event-related potentials recorded subdurally from patients find face-selective responses (larger N200 for faces vs. nonfaces) across a large extent of the fusiform gyrus as well as multiple face-selective regions within a single subject that are separated about 1.5–2.5 cm apart along an anterior/posterior axis (Allison et al., 1999). Overall, previous human and monkey studies do not propose definitive criteria for deciding when activated clusters should be separated or combined. Thus, counting the number of clusters that are face-selective is not a productive method in determining the computations involved in face perception.

Instead we propose that systematic criteria can be employed for defining face- and limb-selective activations using spatial relationships with other category-selective activations and retinotopic regions. Using these combined criteria we are able to show a reliable organization of face-selective patches indicating that there are three face-selective clusters along the IOG and FG and two distinct limb-selective clusters on the ITG and OTS. By using HR-fMRI without spatial smoothing in addition to retinotopy, we provide a method to consistently delineate this series of face- and limb-selective clusters. Particularly, hV4, VO-1/2, and the two limb-selective clusters serve as reliable boundaries among face-selective activations, whereas face-

selective pFus serves as a boundary between the limb-selective ITG and OTS clusters. Having consistent criteria to define activations is important for increasing the generalizability of results across studies with normals as well as patient studies (Dalton et al., 2005; Schiltz et al., 2006) and for enhancing comparisons across species (e.g. human and monkey fMRI). By adding retinotopy scans as well as body part stimuli in localizer experiments, groups can reliably delineate the face- and limb-selective activations.

While there is variability in the location of the face-selective activations, and not all face-selective activations are identified in all subjects, our method reliably delineates activations systematically across subjects. For example, though Subject 4 does not have a face-selective pFus in the left hemisphere (Fig. 4A), we identified the FG activation as 'mFus' rather than 'pFus' due to its relationship to VO-1/2 and the limb-selective OTS. Presently the source of the variability across subjects is not well understood and it may reflect individual differences across human brains. This variability may be exacerbated from a susceptibility artifact induced by the transverse sinus located lateral to hV4. The location of the transverse sinus in a particular brain as well as its orientation compared to the magnetic field in the scanner can produce an artifact that may affect the ability to reliably measure activations along the IOG, pFus, and the limb-selective ITG (Winawer et al., 2010).

A gradient of face processing in ventral temporal cortex

Our findings indicate a gradient of face processing as one ascends ventral temporal cortex from the inferior occipital gyrus to the fusiform gyrus. First, selectivity analyses show that each of the face-selective activations (mFus, pFus, and IOG) responds more strongly to faces relative to the mean across other categories (Figs. 6 and 7A), where the IOG has the lowest selectivity for faces. Second, in quantifying the amount of overlap between face- and limb-selective voxels in each of these activations, the IOG has significantly more overlapping voxels than either FG activation. Third, MVP analyses within each face-selective ROI reveal independent information for faces and limbs in each ROI, with a gradient in the reproducibility of limb-MVPs across these regions (Supplemental Fig. 2). Such findings are suggestive of a hierarchy of face processing where there is likely more general processing in the IOG and increased specialization to faces as one ascends this hierarchy to the mFus (which is the most anterior activation measured with our current high-resolution scanning acquisition).

What do our data reveal about the functional properties of the IOG? First, our data suggest that researchers should take caution when labeling an area as face-selective because this selectivity is relative to the categories used. Without using limb stimuli, this region might appear to be exclusively selective for faces. In the present study, this cluster illustrates limb selectivity (vs. cars and houses) that is comparable to its face selectivity (vs. cars and houses, Fig. 7B). On the other hand, our statistical contrast maps (Fig. 4A — red) and selectivity analyses (Fig. 7A) show significant face selectivity (vs. all categories) in this region. The latter finding is consistent with recent reports indicating the IOG (sometimes referred to as the occipital face area, OFA; Gauthier et al., 2000; Haxby et al., 2000; Pinsk et al., 2009; Schwarzlose et al., 2008) responds more strongly to faces compared to headless bodies (Schwarzlose et al., 2008), and body parts (Pinsk et al., 2009). Second, we found that the distributed responses for faces and limbs are decorrelated within the IOG, indicating that despite similar selectivity for faces and limbs across the mean response of this region, there are distinct representations for faces and limbs at a finer spatial scale than the ROI level. Thus, while previous results indicate the involvement of the IOG in face recognition (Pitcher et al., 2009; Rossion et al., 2003; Sorger et al., 2007), we propose that the IOG is intermediate in the hierarchy of face processing.

Laterality of the spatial organization of face- and limb-selective activations

Past studies in normal subjects report laterality effects of face- and body part-selective activations in both the size of the activation (Allison et al., 1999; Golarai et al., 2007; Kanwisher et al., 1997) and the ability to detect the activation (Kanwisher et al., 1997; Peelen and Downing, 2005), where there is a right hemisphere bias for both size and occurrence. An interesting observation from our data is that the alternating organization among face- and limb-selective clusters tends to be more consistent in the right hemisphere compared to the left hemisphere. That is, the limb-selective OTS activation intervenes between the mFus and pFus face-selective clusters most clearly in the right hemisphere. In the left hemisphere, however, the limb-selective OTS is lateral to the face-selective activations in all subjects, and intervenes between the face-selective clusters in some subjects. Thus, we propose an additional characteristic of laterality — a difference in the spatial organization among face- and limb-selective activations across hemispheres. We speculate that this difference in spatial organization may be in part driven by the opposite laterality effect observed for the visual word form area (VWFA). The VWFA is often located in the posterior fusiform gyrus (Baker et al., 2007; Cohen et al., 2000; Dehaene et al., 2002) or on two OTS locations (Ben-Shachar et al., 2007, for a review) and is more dominant in the left hemisphere. Future research can test this idea by examining the spatial relation among the word form-, face- and body part-selective activations within and across hemispheres.

Implications for delineation of other category-selective regions

Similar methods to the ones we have developed here can be used to improve the precision and consistency of the definition of other category-selective activations within and across studies (e.g. in lateral occipito-temporal cortex, see Supplemental Fig. 1).

Currently, there is a tendency to label regions in a descriptive fashion such as the 'extrastriate body area', 'lateral occipital complex', or 'visual word form area'. A more accurate and consistent nature of functional organization as measured with fMRI in the human and monkey brain can be revealed by (1) making more spatially refined measurements, (2) tracking anatomical locations, and (3) determining the relative spatial organization of category-selective regions relative to other functional regions and visual field maps.

Distributed responses for faces and limbs are anticorrelated with less information about faces in medial compared to lateral VTC

Our MVP analyses complement and extend our GLM analyses both in visualizing the alternating nature of separate clustered activations for faces and limbs, as well as in quantifying the correlation structure of distributed patterns for these categories. First, unthresholded activation maps illustrate that the 'hot spots' for faces and limbs alternate (compare Fig. 4A, Subject 1 with Fig. 8), where the voxels that respond highly for limbs are most consistently clustered lateral and posterior to the fusiform clusters that respond highly to faces in lateral VTC. Thus, localizing this series of face- and limb-selective clusters is not dependent on statistical thresholding and GLM analyses. Even with unthresholded MVPs, it is apparent that different sets of voxels in VTC preferentially respond to faces and limbs. Second, our GLM analyses across thresholds illustrate minimal overlap among face- and limb-selective voxels at all thresholds (Figs. 4B–C). Previous results showing significant overlap are likely due to partial voluming effects induced by larger voxels (>3 mm on a side) as well as analysis methods with spatially smoothed activations. Third, our MVP analyses extend this relationship to indicate that voxels that are weakly selective to limbs or faces outside of the clustered activations (which are not picked up by the GLM analyses) have an anticorrelated

relationship, which is predicted by separate sets of voxels coding each category. Furthermore, our data indicate that this anticorrelated relationship is reproducible across our high-resolution sessions and is specific only to the highly- and weakly-selective voxels in lateral VTC. In fact, we find a different relationship between face and limb MVPs in non-selective voxels in medial VTC where the distributed responses for faces and limbs are decorrelated. This decorrelation contributes to the decrease in classification performance for faces in medial VTC illustrating that this difference in spatial relationship across voxels is indicative of different amounts of information for faces between medial and lateral VTC. Despite this decrease in classification performance, the non-selective voxels in medial VTC can discriminate between animate categories even though there are no voxels selective for either category in this area of cortex.

Taken together, we illustrate that with HR-fMRI and no spatial smoothing, the spatial organization of distributed responses to faces and limbs are anticorrelated in highly- and weakly-selective voxels in lateral VTC, indicating that even weakly-selective, unthresholded distributed responses for faces and limbs are distinct from one another. However, the responses in non-selective voxels are decorrelated. This distinction suggests that there are different amounts of information in the distributed neural code, as well as different spatial relationships between distributed responses in medial and lateral VTC.

Conclusion: sparsely-distributed organization

Our data indicate an interaction between localized cortical clusters and distributed responses across voxels within as well as outside these clusters, suggestive of a sparsely-distributed organization mediating the debate between modular and distributed theories of object representation. Sparseness here refers to the presence of a series of minimally overlapping highly-selective clusters that are arranged in a consistent topography relative to one another as well as early visual areas, while distributed refers to the fact that despite the minimal overlap across clusters, there is substantial (but different) amounts of information in the responses across voxels coding either category. This sparsely-distributed organization is supported by recent cortical connectivity studies indicating a hybrid modular and distributed organization (Borra et al., 2010; Zangenehpour and Chaudhuri, 2005), as well as theoretical work of a sparse-distributed network (Kanerva, 1988).

As scanning resolutions improve for human fMRI studies, the number of clusters is likely to increase, but the alternating nature of face and limb representations is likely to remain in adjacent activations as also suggested by monkey fMRI (Pinsk et al., 2009; Tsao et al., 2003) and optical imaging (Sato et al., 2009). This sparsely-distributed organization brings to question whether category-selectivity is a sufficient criterion to define a brain region. It further suggests that modular and distributed models of object representation should consider how a series of minimally overlapping category-selective clusters that are themselves distributed affect the functional and spatial predictions of each respective model. Future studies of face, body part, and object recognition should therefore examine whether the same or different computations are instantiated in these different clusters and test whether the information within and outside the various clusters is related to performance in specific perceptual tasks.

Acknowledgments

This work was supported by National Eye Institute 1R21EY017741, NSF BCS 0617688, NSF BCS 0920865 and Whitehall Foundation 2005-05-111-RES grants to KGS. We would also like to thank Nick Davidenko, David Remus, Brian Wandell, Jon Winawer, and Nathan Witthoft for fruitful discussions, as well as Janice Chen for technical assistance.

Appendix A. Supplementary data

Supplementary data associated with this article can be found, in the online version, at doi:10.1016/j.neuroimage.2010.04.262.

References

Aguirre, G.K., Zarahn, E., D'Esposito, M., 1998. An area within human ventral cortex sensitive to "building" stimuli: evidence and implications. Neuron 21, 373–383.
Allison, T., Puce, A., Spencer, D.D., McCarthy, G., 1999. Electrophysiological studies of human face perception. I: Potentials generated in occipitotemporal cortex by face and non-face stimuli. Cereb. Cortex 9, 415–430.
Andrews, T.J., Ewbank, M.P., 2004. Distinct representations for facial identity and changeable aspects of faces in the human temporal lobe. Neuroimage 23, 905–913.
Andrews, T.J., Schluppeck, D., Homfray, D., Matthews, P., Blakemore, C., 2002. Activity in the fusiform gyrus predicts conscious perception of Rubin's vase–face illusion. Neuroimage 17, 890–901.
Arcaro, M.J., McMains, S.A., Singer, B.D., Kastner, S., 2009. Retinotopic organization of human ventral visual cortex. J. Neurosci. 29, 10638–10652.
Baker, C.I., Liu, J., Wald, L.L., Kwong, K.K., Benner, T., Kanwisher, N., 2007. Visual word processing and experiential origins of functional selectivity in human extrastriate cortex. Proc. Natl. Acad. Sci. U. S. A. 104, 9087–9092.
Ben-Shachar, M., Dougherty, R.F., Wandell, B.A., 2007. White matter pathways in reading. Curr. Opin. Neurobiol. 17, 258–270.
Borra, E., Ichinohe, N., Sato, T., Tanifuji, M., Rockland, K.S., 2010. Cortical connections to area TE in monkey: hybrid modular and distributed organization. Cereb. Cortex 20 (2), 257–270.
Brainard, D.H., 1997. The psychophysics toolbox. Spat. Vis. 10, 433–436.
Brewer, A.A., Liu, J., Wade, A.R., Wandell, B.A., 2005. Visual field maps and stimulus selectivity in human ventral occipital cortex. Nat. Neurosci. 8, 1102–1109.
Cohen, L., Dehaene, S., Naccache, L., Lehericy, S., Dehaene-Lambertz, G., Henaff, M.A., Michel, F., 2000. The visual word form area: spatial and temporal characterization of an initial stage of reading in normal subjects and posterior split-brain patients. Brain 123 (Pt 2), 291–307.
Cox, D.D., Savoy, R.L., 2003. Functional magnetic resonance imaging (fMRI) "brain reading": detecting and classifying distributed patterns of fMRI activity in human visual cortex. Neuroimage 19, 261–270.
Dalton, K.M., Nacewicz, B.M., Johnstone, T., Schaefer, H.S., Gernsbacher, M.A., Goldsmith, H.H., Alexander, A.L., Davidson, R.J., 2005. Gaze fixation and the neural circuitry of face processing in autism. Nat. Neurosci. 8, 519–526.
Dehaene, S., Le Clec, H.G., Poline, J.B., Le Bihan, D., Cohen, L., 2002. The visual word form area: a prelexical representation of visual words in the fusiform gyrus. NeuroReport 13, 321–325.
Downing, P.E., Wiggett, A.J., Peelen, M.V., 2007. Functional magnetic resonance imaging investigation of overlapping lateral occipitotemporal activations using multi-voxel pattern analysis. J. Neurosci. 27, 226–233.
Dumoulin, S.O., Bittar, R.G., Kabani, N.J., Baker Jr., C.L., Le Goualher, G., Bruce Pike, G., Evans, A.C., 2000. A new anatomical landmark for reliable identification of human area V5/MT: a quantitative analysis of sulcal patterning. Cereb. Cortex 10, 454–463.
Edelman, S., Grill-Spector, K., Kusnir, T., Malach, R., 1998. Towards direct visualization of the internal shape space by fMRI. Psychobiology (special issue on Cognitive Neuroscience of Object Representation and Recognition) 26, 309–321.
Engell, A.D., Haxby, J.V., 2007. Facial expression and gaze-direction in human superior temporal sulcus. Neuropsychologia 45, 3234–3241.
Epstein, R., Kanwisher, N., 1998. A cortical representation of the local visual environment. Nature 392, 598–601.
Felleman, D.J., Van Essen, D.C., 1991. Distributed hierarchical processing in the primate cerebral cortex. Cereb. Cortex 1, 1–47.
Gauthier, I., Skudlarski, P., Gore, J.C., Anderson, A.W., 2000. Expertise for cars and birds recruits brain areas involved in face recognition. Nat. Neurosci. 3, 191–197.
Glover, G.H., 1999. Simple analytic spiral K-space algorithm. Magn. Reson. Med. 42, 412–415.
Golarai, G., Ghahremani, D.G., Whitfield-Gabrieli, S., Reiss, A., Eberhardt, J.L., Gabrieli, J. D., Grill-Spector, K., 2007. Differential development of high-level visual cortex correlates with category-specific recognition memory. Nat. Neurosci. 10, 512–522.
Grill-Spector, K., 2003. The neural basis of object perception. Curr. Opin. Neurobiol. 13, 159–166.
Grill-Spector, K., Kanwisher, N., 2005. Visual recognition: as soon as you know it is there, you know what it is. Psychol. Sci. 16, 152–160.
Grill-Spector, K., Knouf, N., Kanwisher, N., 2004. The fusiform face area subserves face perception, not generic within-category identification. Nat. Neurosci. 7, 555–562.
Grill-Spector, K., Sayres, R., Ress, D., 2006. High-resolution imaging reveals highly selective nonface clusters in the fusiform face area. Nat. Neurosci. 9, 1177–1185.
Hadj-Bouziane, F., Bell, A.H., Knusten, T.A., Ungerleider, L.G., Tootell, R.B., 2008. Perception of emotional expressions is independent of face selectivity in monkey inferior temporal cortex. Proc. Natl. Acad. Sci. U. S. A. 105, 5591–5596.
Halgren, E., Dale, A.M., Sereno, M.I., Tootell, R.B., Marinkovic, K., Rosen, B.R., 1999. Location of human face-selective cortex with respect to retinotopic areas. Hum. Brain Mapp. 7, 29–37.
Hanson, S.J., Halchenko, Y.O., 2008. Brain reading using full brain support vector machines for object recognition: there is no "face" identification area. Neural Comput. 20, 486–503.
Hasson, U., Hendler, T., Ben Bashat, D., Malach, R., 2001. Vase or face? A neural correlate of shape-selective grouping processes in the human brain. J. Cogn. Neurosci. 13, 744–753.

Haxby, J.V., Hoffman, E.A., Gobbini, M.I., 2000. The distributed human neural system for face perception. Trends Cogn. Sci. 4, 223–233.
Haxby, J.V., Gobbini, M.I., Furey, M.L., Ishai, A., Schouten, J.L., Pietrini, P., 2001. Distributed and overlapping representations of faces and objects in ventral temporal cortex. Science 293, 2425–2430.
Hoffman, K.L., Gothard, K.M., Schmid, M.C., Logothetis, N.K., 2007. Facial-expression and gaze-selective responses in the monkey amygdala. Curr. Biol. 17, 766–772.
Ishai, A., Ungerleider, L.G., Martin, A., Haxby, J.V., 2000. The representation of objects in the human occipital and temporal cortex. J. Cogn. Neurosci. 12 (Suppl 2), 35–51.
Kanerva, P., 1988. Sparse Distributed Memory. MIT Press, Cambridge, MA.
Kanwisher, N., 2000. Domain specificity in face perception. Nat. Neurosci. 3, 759–763.
Kanwisher, N., McDermott, J., Chun, M.M., 1997. The fusiform face area: a module in human extrastriate cortex specialized for face perception. J. Neurosci. 17, 4302–4311.
Kriegeskorte, N., Formisano, E., Sorger, B., Goebel, R., 2007. Individual faces elicit distinct response patterns in human anterior temporal cortex. Proc. Natl. Acad. Sci. U. S. A. 104, 20600–20605.
Kruger, G., Glover, G.H., 2001. Physiological noise in oxygenation-sensitive magnetic resonance imaging. Magn. Reson. Med. 46, 631–637.
Logothetis, N.K., Guggenberger, H., Peled, S., Pauls, J., 1999. Functional imaging of the monkey brain. Nat. Neurosci. 2, 555–562.
Moeller, S., Freiwald, W.A., Tsao, D.Y., 2008. Patches with links: a unified system for processing faces in the macaque temporal lobe. Science 320, 1355–1359.
Nestares, O., Heeger, D.J., 2000. Robust multiresolution alignment of MRI brain volumes. Magn. Reson. Med. 43, 705–715.
Op de Beeck, H.P., Haushofer, J., Kanwisher, N.G., 2008. Interpreting fMRI data: maps, modules and dimensions. Nat. Rev. Neurosci. 9, 123–135.
Peelen, M.V., Downing, P.E., 2005. Selectivity for the human body in the fusiform gyrus. J. Neurophysiol. 93, 603–608.
Peelen, M.V., Downing, P.E., 2007a. The neural basis of visual body perception. Nat. Rev. Neurosci. 8, 636–648.
Peelen, M.V., Downing, P.E., 2007b. Using multi-voxel pattern analysis of fMRI data to interpret overlapping functional activations. Trends Cogn. Sci. 11, 4–5.
Peelen, M.V., Wiggett, A.J., Downing, P.E., 2006. Patterns of fMRI activity dissociate overlapping functional brain areas that respond to biological motion. Neuron 49, 815–822.
Pinsk, M.A., DeSimone, K., Moore, T., Gross, C.G., Kastner, S., 2005. Representations of faces and body parts in macaque temporal cortex: a functional MRI study. Proc. Natl. Acad. Sci. U. S. A. 102, 6996–7001.
Pinsk, M.A., Arcaro, M., Weiner, K.S., Kalkus, J.F., Inati, S.J., Gross, C.G., Kastner, S., 2009. Neural representations of faces and body parts in macaque and human cortex: a comparative FMRI study. J. Neurophysiol. 101, 2581–2600.
Pitcher, D., Charles, L., Devlin, J.T., Walsh, V., Duchaine, B., 2009. Triple dissociation of faces, bodies, and objects in extrastriate cortex. Curr. Biol. 19, 319–324.
Puce, A., Allison, T., Bentin, S., Gore, J.C., McCarthy, G., 1998. Temporal cortex activation in humans viewing eye and mouth movements. J. Neurosci. 18, 2188–2199.
Rajimehr, R., Young, J.C., Tootell, R.B., 2009. An anterior temporal face patch in human cortex, predicted by macaque maps. Proc. Natl. Acad. Sci. U. S. A. 106, 1995–2000.
Rossion, B., Caldara, R., Seghier, M., Schuller, A.M., Lazeyras, F., Mayer, E., 2003. A network of occipito-temporal face-sensitive areas besides the right middle fusiform gyrus is necessary for normal face processing. Brain 126, 2381–2395.
Sato, T., Uchida, G., Tanifuji, M., 2009. Cortical columnar organization is reconsidered in inferior temporal cortex. Cereb. Cortex 19 (8), 1870–1888.
Sayres, R., Grill-Spector, K., 2008. Relating retinotopic and object-selective responses in human lateral occipital cortex. J. Neurophysiol. 100, 249–267.
Schiltz, C., Sorger, B., Caldara, R., Ahmed, F., Mayer, E., Goebel, R., Rossion, B., 2006. Impaired face discrimination in acquired prosopagnosia is associated with abnormal response to individual faces in the right middle fusiform gyrus. Cereb. Cortex 16, 574–586.
Schwarzlose, R.F., Baker, C.I., Kanwisher, N., 2005. Separate face and body selectivity on the fusiform gyrus. J. Neurosci. 25, 11055–11059.
Schwarzlose, R.F., Swisher, J.D., Dang, S., Kanwisher, N., 2008. The distribution of category and location information across object-selective regions in human visual cortex. Proc. Natl. Acad. Sci. U. S. A. 105, 4447–4452.
Sorger, B., Goebel, R., Schiltz, C., Rossion, B., 2007. Understanding the functional neuroanatomy of acquired prosopagnosia. Neuroimage 35, 836–852.
Spiridon, M., Kanwisher, N., 2002. How distributed is visual category information in human occipito-temporal cortex? An fMRI study. Neuron 35, 1157–1165.
Spiridon, M., Fischl, B., Kanwisher, N., 2006. Location and spatial profile of category-specific regions in human extrastriate cortex. Hum. Brain Mapp. 27, 77–89.
Tong, F., Nakayama, K., Vaughan, J.T., Kanwisher, N., 1998. Binocular rivalry and visual awareness in human extrastriate cortex. Neuron 21, 753–759.
Tsao, D.Y., Freiwald, W.A., Knutsen, T.A., Mandeville, J.B., Tootell, R.B., 2003. Faces and objects in macaque cerebral cortex. Nat. Neurosci. 6, 989–995.
Tsao, D.Y., Moeller, S., Freiwald, W.A., 2008. Comparing face patch systems in macaques and humans. Proc. Natl. Acad. Sci. U. S. A. 105, 19514–19519.
Weiner, K.S., Sayres, R., Vinberg, J., Grill-Spector, K., 2010. fMRI-adaptation and category selectivity in human ventral temporal cortex: regional differences across time scales. J. Neurophysiol. 103.
Winawer, J., Horiguchi, H., Sayres, R.A., Amano, K., Wandell, B.A., 2010. Mapping hV4 and ventral occipital cortex: the venous eclipse. Journal of Vision 10 (5), article 1.
Worsley, K.J., Poline, J.B., Friston, K.J., Evans, A.C., 1997. Characterizing the response of PET and fMRI data using multivariate linear models. Neuroimage 6, 305–319.
Zangenehpour, S., Chaudhuri, A., 2005. Patchy organization and asymmetric distribution of the neural correlates of face processing in monkey inferotemporal cortex. Curr. Biol. 15, 993–1005.